Supporting Information for

Electrogenerated Chemiluminescence Imaging of Plasmon-Induced Electrochemical Reaction at Single Nanocatalysts

Qian-Qian Tao, [a] ‡ Cong-Hui Xu, [b] ‡ Wei Zhao, * [b] Hong-Yuan Chen [a] and Jing-Juan Xu *[a]

a Q. Tao, Prof. C. Xu, Prof. W. Zhao, Prof. H. Chen, Prof. J. Xu
State Key Laboratory of Analytical Chemistry for Life Science and Collaborative Innovation Center of Chemistry for Life Sciences, School of Chemistry and Chemical Engineering
Nanjing University
Nanjing 210023, China
E-mail: xujj@nju.edu.cn

b Prof. W. Zhao, Prof. C. Xu,
Institute of Nanochemistry and Nanobiology, School of Environmental and Chemical Engineering
Shanghai University
Shanghai 200444, China
Email: wei_zhao@shu.edu.cn

‡ These authors contributed equally.

Table of contents

1. Reagents and materials.

Gold nanoparticles with average diameters of 60 nm, 80 nm, 100 nm, 200 nm were purchased from Ted Pella, Inc, with surface stabilized by citrate. 3-Aminopropyl triethoxysilane (APTES, 99%), Chloroplatinic acid ($H_2PtCl_6 \cdot xH_2O$, ≥99.9% trace metals basis) and L-ascorbic acid (AA) were obtained from Sigma-Aldrich (U.S.A). 8-Amino-5-chloro-7-phenylpyrido[3,4-d]-pyridazine-1,4[2H,3H]-dione (L-012, a luminol analogue) was bought from Wako Chemical U.S.A., Inc. (Richmond, VA). H_2O_2 (30%) were obtained from Sinopharm Chemical Reagent. 1 M Tris-HCl buffer solution (pH 8.0) was purchased from KeyGEN Biotech (Nanjing, China). Indium tin oxide (ITO)-coated glass slides (coating thickness, ~100 nm; resistance, ~10 Ω/square) were purchased from CSG (Shenzhen, China). Millipore water (Millipore, Inc., Bedford, MA) treated with 0.22 μm filter (PES membrane, Merck Millipore Ltd) was used throughout the experiments.

2. Synthesis of Au@Pt NPs with different Pt shell thicknesses.

The synthesis of Au@Pt core-shell nanoparticles (Au@Pt NPs) was based on previous work with some minor modifications[1]. Briefly, Au NP seed solution with a diameter of 80 nm was centrifuged, washed and dispersed in ultrapure water before use. Firstly, 200 μL of H_2PtCl_6 (3.86 mM) was added to a clean flask containing 5 mL of Au NP seed solution, and then heated to 80°C with magnetic stirring. Next, a 400 μL aliquot of 10 mM ascorbic acid was slowly dropped into this mixture in 3 min with a syringe. Afterwards the mixture was heated and stirred for another 30 min. The diameter of obtained Au@Pt NPs was determined by TEM to be around 100 nm and the thickness of Pt shell was 10 nm. Similar to the steps above, Au@Pt NPs with Pt shell thickness of 5 nm and 20 nm were prepared with 100, 300 μL of H_2PtCl_6 and 200, 600 μL of ascorbic acid solution, respectively.

3. Apparatus for characterization.

The morphologies of Au NPs and Au@Pt NPs were characterized using JEOL200CX transmission electron microscopy (TEM) operated at 200kV. EDX High-angle annular dark field (HAADF) STEM and STEM-EDX elemental mapping was achieved on JEM-2100F (JEOL Ltd., Japan). Scanning electron microscopy (SEM) images were acquired using a Hitachi S4800 (JEOL Ltd., Japan) operating at beam voltages of 5-15 KV. UV–vis adsorption spectroscopic characterization was performed using a Nanodrop-2000C spectrophotometer (Thermo Fisher Scientific Inc.). Traditional electrochemical measurements were performed using CHI-600E (CH Instruments Ins.) and MPI-E multifunctional electrochemical and chemiluminescent analytical system (Xi'an Remax Electronic Science &Technology Co. Ltd., Xi'an, China) with three-electrode system at room temperature. Apparatus for characterization.

4. Dark-field microscopy (DFM) and ECL setup.

Dark-field images were carried out using inverted microscopy (IX73, Olympus), equipped with a dark-field condenser (0.8 < NA < 0.92) and a 60X objective lens (NA 0.75). Olympus true-color digital camera DP80 were used to capture dark-field image and the scattering spectrum was obtained with a monochromator (Acton SP2358, PI, USA) (grating density: 300 lines/mm; blazed wavelength: 500 nm) combined with liquid nitrogen cooled PyLoN CCD cameras (Princeton Instruments (PI), USA). The ECL microscopy setup was based on DFM. A CHI-600E electrochemical workstation was applied to control the ECL reactions. An electron multiplying CCD (EMCCD) (Andor iXon Ultra 888) with exposure time of 1s was trigged synchronously with CHI 600E by a digital delay/pulse generator. The Ag/AgCl and Pt wire (0.5 mm diameter) were used as the reference and counter electrodes. ITO with samples immobilized on its surface was used as working electrode. The electrolyte was 150 μL 1 M Tris-HCl buffer containing 5 mM L-012 and 50 mM H_2O_2. 532 nm CW laser beam (MGL-FN-532-300 mW) was used to excite the plasmon of Au NP and Au@Pt NP preferentially with different luminous intensity and a 532 nm notch filter (ZET532NF-532, Chroma) was utilized before collecting the ECL image.

5. ECL pathway of L-012-H_2O_2 system.

Charge transfer reactions[2, 3]

$$LH^{-} \rightarrow L^{\cdot -} + e^{-} + H^{+} \tag{1}$$

$$H_2O_2 \rightarrow O_2 + 2H^{+} + 2e^{-} \tag{2}$$

Homogeneous Reactions

$$L^{\cdot -} + O_2 \rightarrow O_2^{\cdot -} + L \tag{3}$$

$$L^{\cdot -} + O_2^{\cdot -} \rightarrow LO_2^{2-} \tag{4}$$

$$LO_2^{2-} \rightarrow AP^{2^-} + N_2 + hv \tag{5}$$

AP^{2-} is on behalf of L-012 gets two oxygen atoms and loses two nitrogen atoms. L stands for L-012.

6. Calculation of the difference in ECL intensity (ΔECL) ratio.

All the ECL intensities depicted in the figures and the data analysis under irradiation were meticulously performed with background correction. $ECL_{laser\ off}$ is the average analog-to-digital (A/D) counts obtained from ECL bright spot before laser irradiation, and an average A/D counts of ten pixels from the area without nanoparticles is calculated as $Background_{laser\ off}$. The subtraction of the two is the ECL intensity of individual particle after background correction. ΔECL is the amount of change in the ECL intensity of the individual particles from laser off to laser on, where the calculation method of $ECL_{laser\ on}$ and $Background_{laser\ on}$ is the same as that of $ECL_{laser\ off}$ and $Background_{laser\ on}$. The computation of $\Delta ECL\ ratio$ is elaborated upon as follows:

$$\Delta ECL\ ratio = \frac{(ECL_{laser\ on} - Background_{laser\ on}) - (ECL_{laser\ off} - Background_{laser\ off})}{ECL_{laser\ off} - Background_{laser\ off}}$$

7. Characterizations of Au NPs with different diameters.

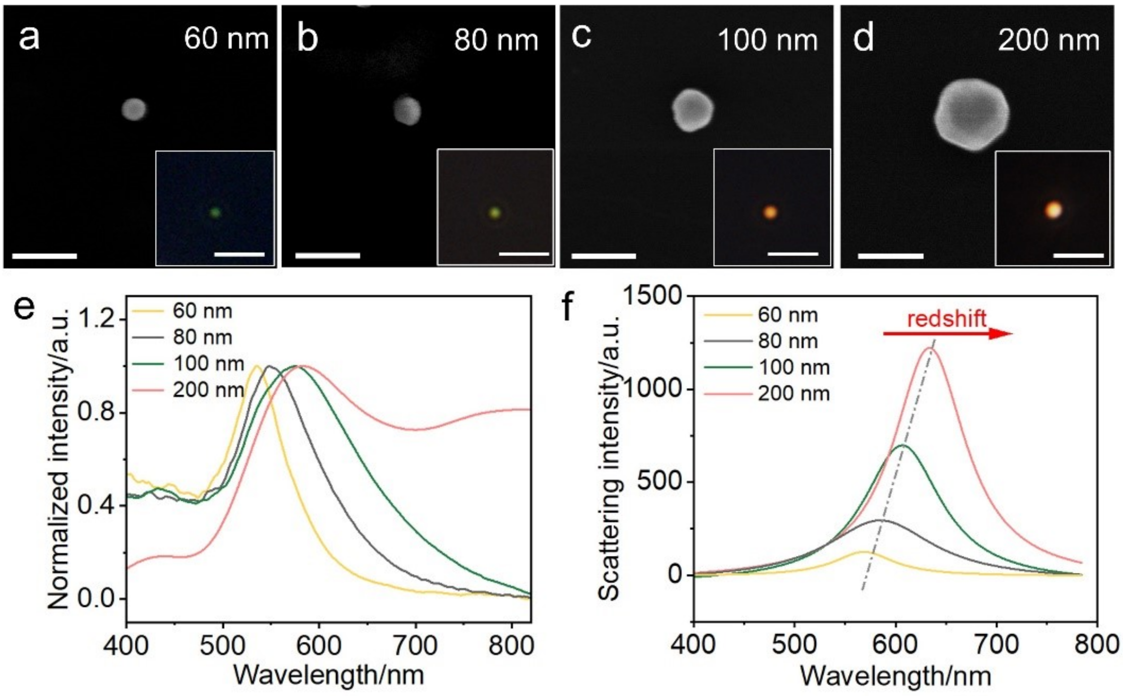

Fig. S1 (a-d) SEM images of Au NPs with different sizes (60, 80, 100, 200 nm). Inset of (a-d) top right: DFM images of the corresponding Au NPs. Scale bar: 5 μm. (e) SPR absorption spectra and (f) Lorentz-fitted scattering spectra of Au NPs with different sizes.

8. ECL of Au NPs with different diameters.

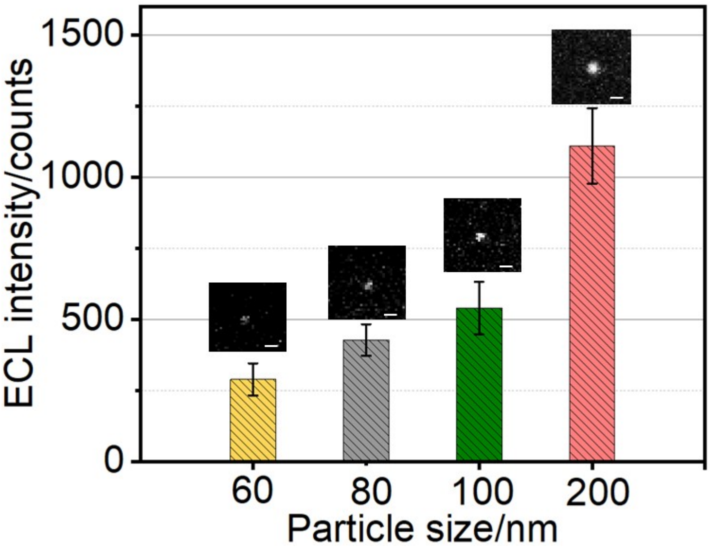

Fig. S2 ECL intensity of Au NPs with different diameters (60, 80, 100, 200 nm). Inset of: ECL images of the single corresponding Au NPs. Scale bar: 1 μm.

9. Morphology characterization of Au@Pt NPs with different Pt shell thicknesses.

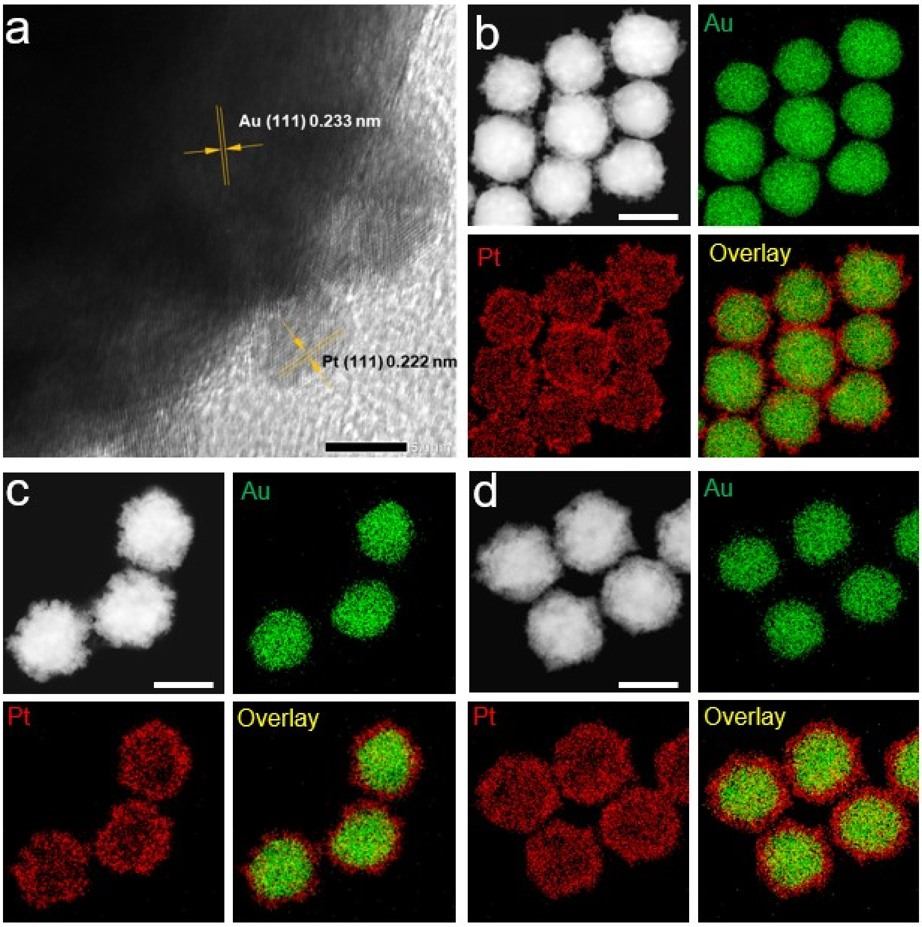

Fig. S3 (a) HR-TEM image of single Au@Pt NP with Pt shell thickness of 5 nm. Scale bar: 5 nm. (b–c)

EDX high-angle annular dark field (HAADF) STEM image and corresponding EDX elemental mapping of Au@Pt NPs with Pt shell thickness of 5 nm, 10 nm and 20 nm. Scale bar: 100 nm.

10. Dark-field images and the corresponding ECL images of Au@Pt NPs and Au NPs.

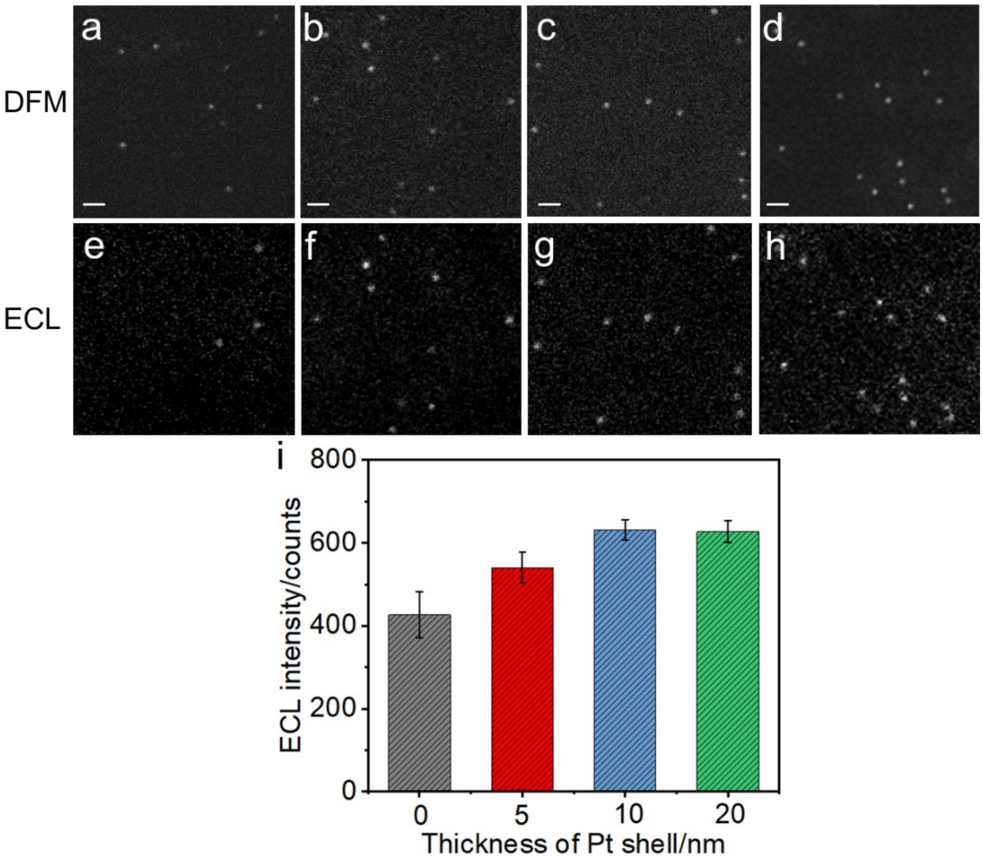

Fig. S4 Dark-field images and the corresponding ECL images of (a, e) Au NPs, Au@Pt NPs with shell thickness of (b, f) 5 nm, (c, g) 10 nm and (d, h) 20 nm at the potential of 0.6 V *vs.* Ag/AgCl. (i) ECL intensity of Au@Pt NPs with different Pt shell thicknesses. All samples for ECL imaging were immersed in 1M Tris-HCl buffer containing 5 mM L-012 and 50 mM H_2O_2 at pH 8.0. Scale bar: 5 μm.

11. UV-vis absorption, fluorescence and ECL characterization of L-012.

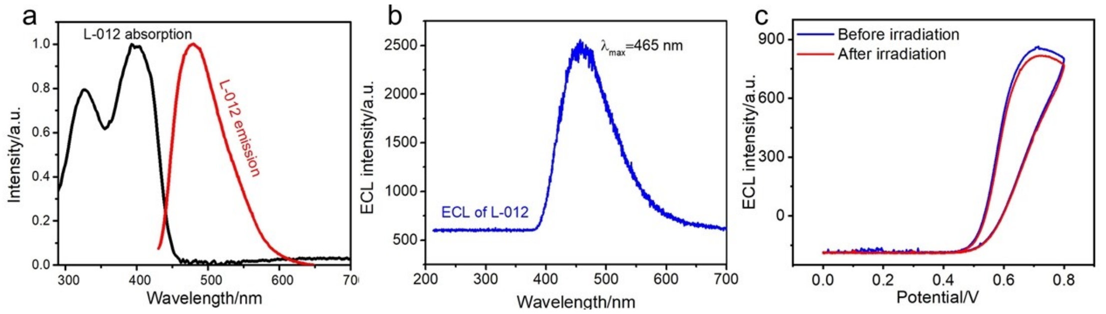

Fig. S5 (a) UV-vis absorption and fluorescence emission spectra, (b) ECL emission spectrum of L-012 and (c) ECL intensity of L-012 solution before and after irradiation of 532 nm laser at 172.72 mW·cm^{-2} for 10 min. The electrolyte is 1 M Tris-HCl buffer (pH= 8.0) containing 1 mM L-012 and 10 mM H_2O_2. Scan rate: 20 mV/s, PMT: 100V.

12. DFM and ECL images of Au NPs with laser OFF or ON.

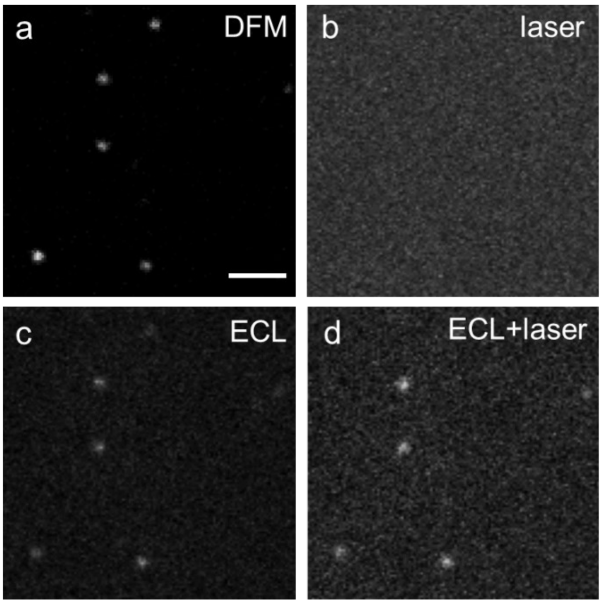

Fig. S6 (a) DFM image of 80 nm Au NPs on ITO. (b) Image of the corresponding area in (a) under 532 nm laser irradiation. (c) ECL image of the corresponding area in (a) under an applied potential of 0.6 V. (d) ECL image under 532 nm laser irradiation. Scale bar: 5 μm. The laser power density used was 172.72 mW·cm^{-2}.

13. Background signal with different power densities.

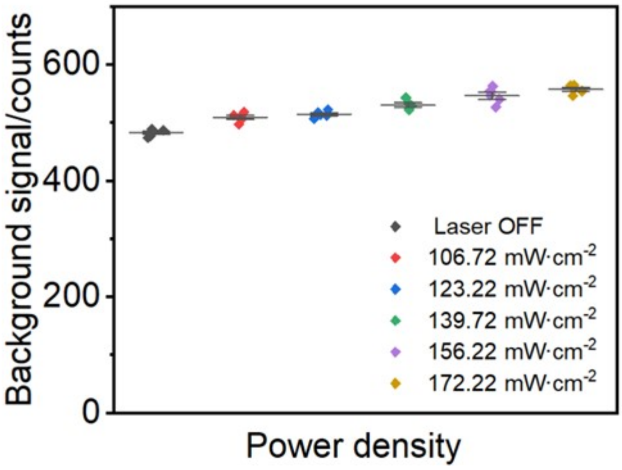

Fig. S7 Background signal under 532 nm laser irradiation with different power densities.

14. Linear sweep voltammetry (LSV) curves with irradiation laser OFF and ON.

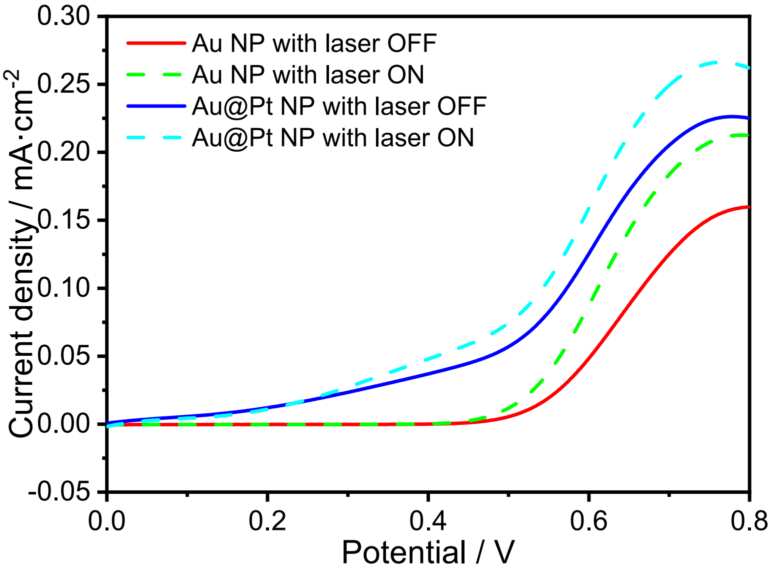

Fig. S8 The Linear sweep voltammetry (LSV) curves on Au NPs- or Au@Pt NPs-modified ITO electrode with or without illumination of 532 nm-wavelength laser at the 172.72 mW·cm^{-2}. The electrolyte is 1 M Tris-HCl buffer (pH= 8.0) containing 1 mM L-012 and 10 mM H_2O_2. Scan rate: 20 mV/s.

15. Statistical analysis of ECL intensity as a function laser power density.

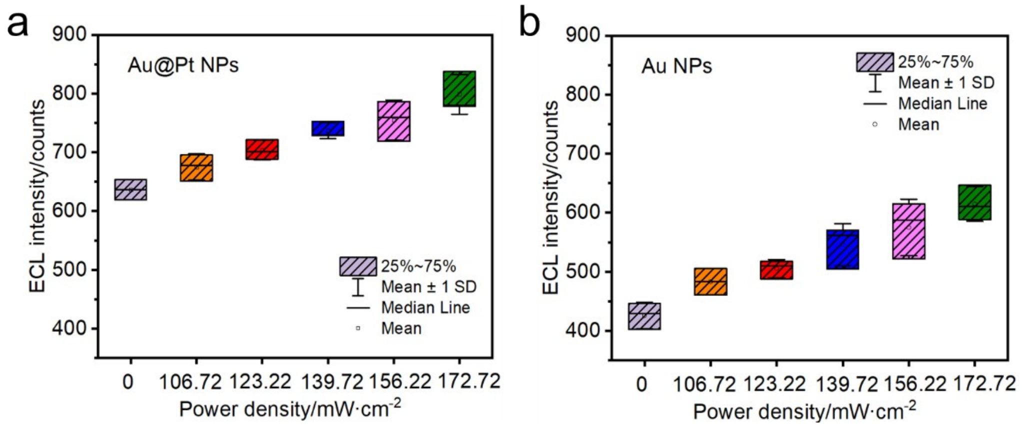

Fig. S9 Statistical analysis of ECL intensity on (a) Au@Pt NPs with a 10 nm Pt shell and (b) Au NPs as a function laser power density.

16. Statistical analysis of plasmon-induced ECL at individual Au@Pt NPs with shell thickness of 5 nm.

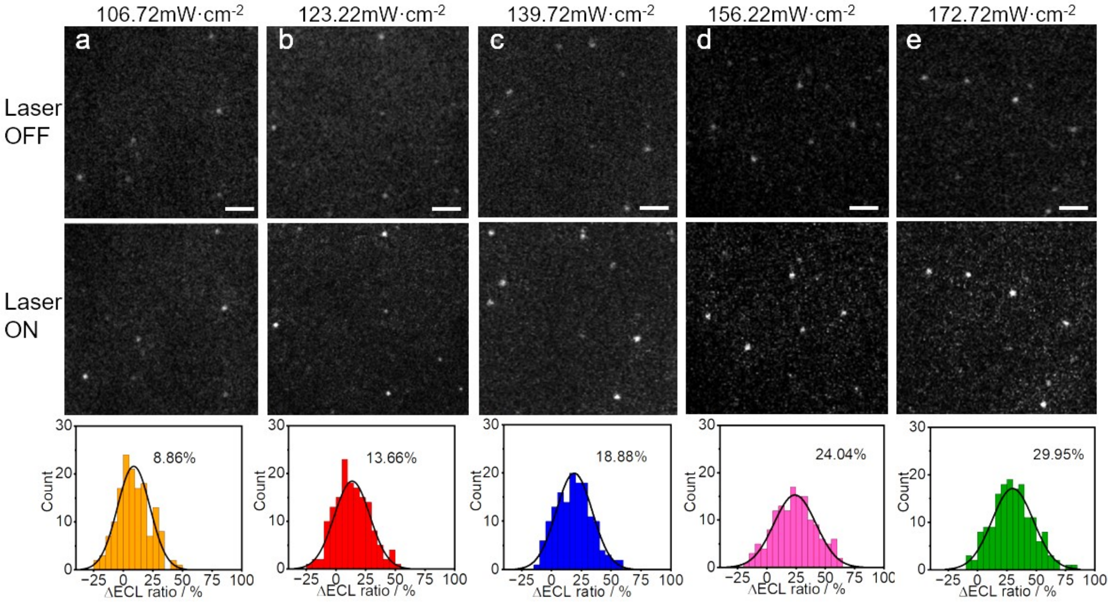

Fig. S10 Top: ECL images of individual Au@Pt NPs with shell thickness of 5 nm with and without 532 nm laser irradiation with power density of (a) 106.72 mW·cm^{-2}, (b) 123.22 mW·cm^{-2}, (c) 139.72 mW·cm^{-2}, (d) 156.22 mW·cm^{-2}, and (e) 172.72 mW·cm^{-2}. Scale bar: 5 μm. Bottom: Corresponding statistical analysis of the distributions of ECL intensities at individual Au@Pt NPs under laser irradiation with different power densities.

17. Statistical analysis of plasmon-induced ECL at individual Au@Pt NPs with shell thickness of 20 nm.

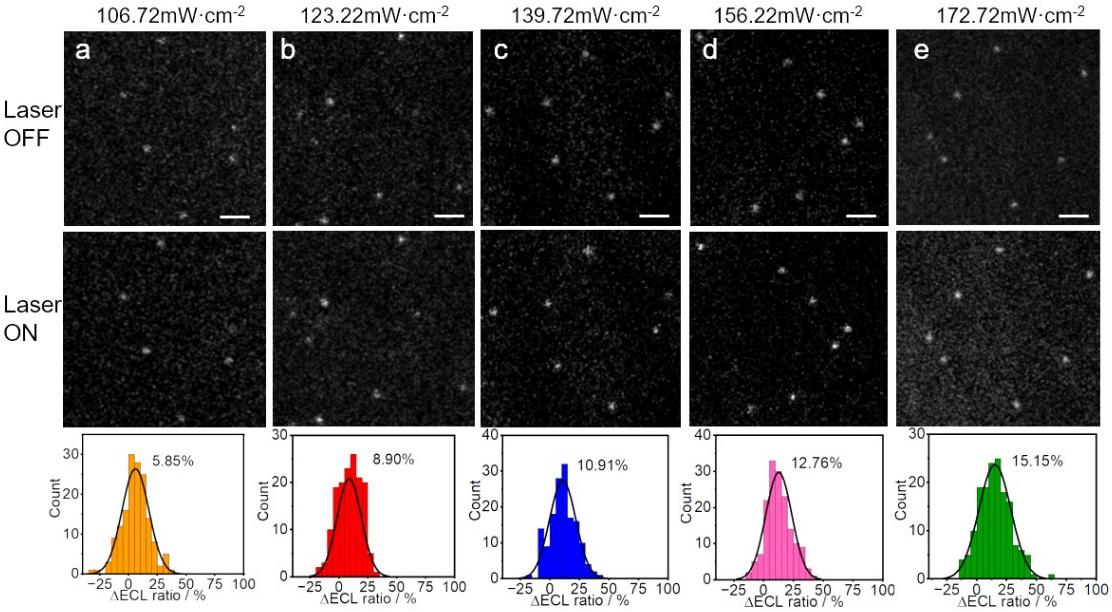

Fig. S11 Top: ECL images of individual Au@Pt NPs with shell thickness of 20 nm with and without 532 nm laser irradiation with power density of (a) 106.72 mW·cm^{-2}, (b) 123.22 mW·cm^{-2}, (c) 139.72 mW·cm^{-2}, (d) 156.22 mW·cm^{-2}, and (e) 172.72 mW·cm^{-2}. Scale bar: 5 μm. Bottom: Corresponding statistical analysis of the distributions of ECL intensities at individual Au@Pt NPs under laser irradiation with different power densities.

18. References

(1) Zhu, Z.; Guan, Z.; Jia, S.; Lei, Z.; Lin, S.; Zhang, H.; Ma, Y.; Tian, Z. Q.; Yang, C. J. Au@Pt nanoparticle encapsulated target-responsive hydrogel with volumetric bar-chart chip readout for quantitative point-of-care testing. *Angew. Chem. Int. Ed. Engl.* **2014**, *53* (46), 12503-12507.

(2) Chen, Y.; Zhao, D.; Fu, J.; Gou, X.; Jiang, D.; Dong, H.; Zhu, J. J. In Situ Imaging Facet-Induced Spatial Heterogeneity of Electrocatalytic Reaction Activity at the Subparticle Level via Electrochemiluminescence Microscopy. *Anal. Chem.* **2019**, *91* (10), 6829-6835.

(3) Chen, M. M.; Xu, C. H.; Zhao, W.; Chen, H. Y.; Xu, J. J. Observing the structure-dependent electrocatalytic activity of bimetallic Pd-Au nanorods at the single-particle level. *Chem. Commun.* **2020**, *56* (23), 3413-3416.